# HOLE EXPANSION SIMULATION CONSIDERING THE DIFFERENTIAL HARDENING OF A SHEET METAL

TOSHIHIKO KUWABARA[1], KAZUHIRO ICHIKAWA[2]

*Abstract*. The effects of material models on the predictive accuracy of the finite element analyses of hole expansion forming are investigated. The test material used is a zinc-coated low carbon steel sheet. Biaxial tensile tests of the test material are performed using cruciform specimens and the multiaxial tube expansion test method to determine proper material models for the test material. The material models used in the FEA are the isotropic hardening (IH) models based on the von Mises, Hill's quadratic, and the Yld2000-2d (Barlat, *et al*., 2003) yield functions, in addition to the differential hardening (DH) model based on the Yld2000-2d yield function (Yld2000-2d (DH)). The Yld2000-2d (DH) yield function gives the most accurate description of the biaxial deformation behavior of the test material. However, even the Yld2000-2d (DH) yield function could not accurately reproduce a tendency of the thickness strain ( $\varepsilon_z^p$ ) distribution in the vicinity of the hole edge. It is concluded that a material model that accurately reproduces the anisotropic deformation behavior of the test material for a stress range from uniaxial tension to plane strain tension along the RD, 45°, and TD should be used in the FEA to improve the predictive accuracy for the $\varepsilon_z^p$ distribution in the vicinity of the hole edge.

*Key words:* sheet metal forming, hole expansion, finite element analysis, low carbon steel sheet, anisotropy, yield function, differential hardening.

## 1. INTRODUCTION

The establishment of trial-and-error-less manufacturing has been strongly desired in industry to shorten the product development period and reduce costs for prototype manufacturing. Improvement of the predictive accuracy for defect formation using finite element analysis (FEA) is a key to realize trial-and-error-less

[1] Department of Mechanical Systems Engineering, Graduate School of Engineering, Tokyo University of Agriculture and Technology, 2-24-16, Nakacho, Koganei-shi, Tokyo, Japan, E-mail: 50014643008@st.tuat.ac.jp

[2] Division of Advanced Mechanical Systems Engineering, Institute of Engineering, Tokyo University of Agriculture and Technology, 2-24-16, Nakacho, Koganei-shi, Tokyo, Japan, E-mail: kuwabara@cc.tuat.ac.jp

Ro. J. Techn. Sci. – Appl. Mechanics, Vol. 60, N$^{os}$ 1–2, P.63–81, Bucharest, 2015

manufacturing. One of the important factors that affect the accuracy of FEA is a material model. In sheet metal forming processes, metal sheets are subjected to various multiaxial stress states. Therefore, the validity of the constitutive equations used in the FEA should be checked by multiaxial stress tests [1].

There have been many studies on numerical analyses of stretch-flanging based on anisotropic yield functions. Parmar and Mellor [2] investigated the plastic deformation of an annulus of sheet metal subjected to a radial tension at its outer periphery using Hill's nonquadratic yield function [3]. Takuda *et al*. [4] investigated the forming limit of hole expansion with a combined use of Hill's quadratic yield function [5] and ductile fracture criterion with the assumption of planar isotropy. Worswick and Finn [6] carried out the FEA and experiment of stretch-flanging of 5000-series aluminum alloy sheet using cylindrical and square punches and concluded the superiority of the Yld89 yield function [7] to the von Mises [8] and Hill's quadratic yield functions. However, no experimental validation was reported for the material models used in these numerical analyses. Therefore, it is still questionable how accurately these numerical analyses capture the real deformation behavior that occurs during stretch-flanging and hole expansion forming.

Kuwabara and coworkers developed a biaxial tensile testing method for sheet metals using cruciform specimens [9, 10]. It has been verified that the material models determined using this testing method are effective for improving the predictive accuracy of the FEA simulations for automotive outer panel forming [11], hydraulic bulge forming [12], and hole expansion forming [13, 14]. However, one of the drawbacks of this testing method is that the maximum plastic strain ranges for which biaxial stress-strain curves of sheet samples can be measured are several percent at most. In order to measure the biaxial stress-strain curves of sheet metals for higher strain ranges the author's research group has developed the multiaxial tube expansion testing method (MTET). A sheet material is bent into a cylindrical shape and the sheet edges are laser-welded together to fabricate a tubular specimen, and then combined internal pressure and tension are applied to the tubular specimen using a servo-controlled tube bulge testing machine developed by Kuwabara *et al*. [15]. The MTET was successfully applied to a measurement of the work hardening behavior of a pure titanium sheet to a maximum plastic strain of 0.085 [16]. The MTET was also effective to measure the forming limit stresses and strains of a cold rolled ultralow carbon steel sheet [17] and a high strength steel sheet [18] under precisely controlled linear stress paths. Yanaga et al. [19] proposed a method of making a differential hardening (DH) model for reproducing the deformation behavior of a 6016-T4 aluminum alloy sheet under biaxial tension from the data of contours of plastic work measured using the MTET and verified that the new constitutive model is effective for improving the accuracy of a FEA for a hydraulic bulge forming.

The objective of this study is to further advance knowledge on the effect of material modelling on the predictive accuracy of FEA. Biaxial tensile tests of a zinc-coated low carbon steel sheet were performed using cruciform specimens and the MTET to determine isotropic hardening (IH) models and a DH model proper to the test material. These material models were then applied to FEAs of hole expansion forming to compare calculated results with experimental data. The effects of the material models on the predictive accuracy of the FEA of hole expansion forming were discussed.

## 2. EXPERIMENTAL METHODS

### 2.1. TEST MATERIAL

The material used was a 0.66 mm thick zinc-coated low carbon steel sheet (SPCD). The work hardening characteristics and *r*-values at 0, 45 and 90° to the rolling direction are listed in Table 1. Hereafter, the rolling direction (RD), transverse direction (TD), and thickness direction of the test material are defined as the *x*-, *y*-, and *z*-axes, respectively.

*Table 1*

Mechanical properties of the test material

| Tensile direction from RD / ° | $\sigma_{0.2}$ / MPa | $c^*$ / MPa | $n^*$ | $\alpha^*$ | *r*-value** |
|---|---|---|---|---|---|
| 0 | 158 | 541 | 0.25 | 0.004 | 1.3 |
| 45 | 162 | 550 | 0.26 | 0.005 | 1.1 |
| 90 | 159 | 535 | 0.26 | 0.005 | 1.5 |

*Approximated using $\sigma = c(\alpha + \varepsilon^{\mathrm{p}})^n$ for $\varepsilon^{\mathrm{p}} = 0.002 \sim 0.248$ (0°), 0.254 (45°), 0.259 (90°).

**Measured at a nominal strain of 0.1.

### 2.2. SPECIMENS FOR BIAXIAL STRESS TESTS

Two types of biaxial tensile tests were performed to measure the plastic deformation behavior of the test material from yielding to fracture. Figure 1a shows a schematic of the cruciform specimen used for the biaxial tensile tests of the as-received sheet sample. The geometry of the specimen was the same as that developed by Kuwabara *et al*. [9, 10], and has been adopted as an international standard [20]. The specimen arms were parallel to the RD and TD of the material. Each arm of the specimen had seven slits, 60 mm long and 0.2 mm wide, at 7.5 mm intervals, to exclude geometric constraint on the deformation of the 60×60 mm$^2$ square gauge area. The slits were fabricated by laser cutting. Normal strain

components ($\varepsilon_x, \varepsilon_y$) were measured using uniaxial strain gauges (YFLA-2, Tokyo Sokki Kenkyujo Co.) mounted at $\pm 21$ mm from the center along the maximum loading direction. According to a FEA of the cruciform specimen with the strain measurement position shown in Fig. 1a, the stress measurement error was estimated to be less than 2% [21, 22]. Details of the biaxial testing apparatus and testing method are given by Kuwabara *et al*. [9, 10].

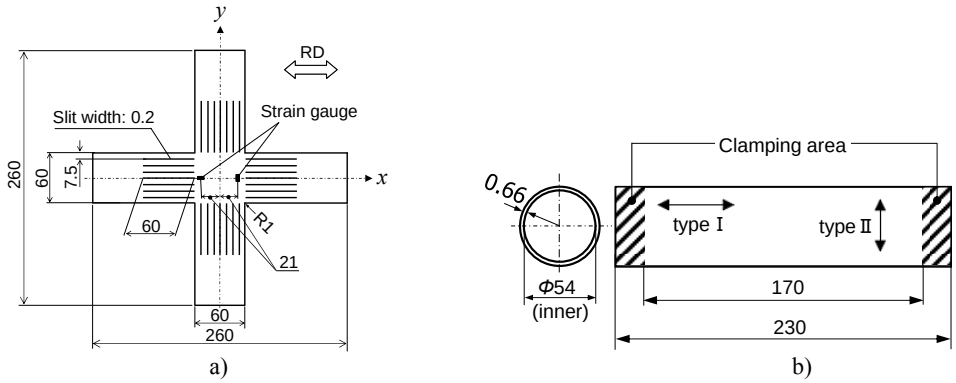


Fig. 1 – Schematic diagrams of specimens used for the biaxial tensile tests (dimensions in mm): a) cruciform specimen; b) tubular specimen. ↔ indicates the RD of the as-received sheet sample.

Figure 1b shows a schematic of the tubular specimen used for the multiaxial tube expansion tests. The specimens were fabricated by bending the sheet samples into a cylindrical shape and laser-welding the sheet edges together to produce an inner diameter of 54 mm and a gauge length (distance between the clamping jigs) of 170 mm. Two types of tubular specimens were fabricated; type I specimens had the RD in the axial direction and type II specimens had the RD in the circumferential direction. Type I specimens were used for tests with $\sigma_x < \sigma_y$ and type II for tests with $\sigma_x \geq \sigma_y$; the maximum principal stress direction was always taken to be in the circumferential direction. Details of the multiaxial tube expansion testing apparatus and testing method are given in Kuwabara and Sugawara (2013) [17].

## 2.3 BIAXIAL STRESS TESTS

Both cruciform and tubular specimens were subjected to proportional loading paths with the true stress ratios $\sigma_x : \sigma_y = 4{:}1$, 2:1, 4:3, 1:1, 3:4, 1:2 and 1:4. Standard uniaxial tensile specimens (JIS 13 B-type) were used for the uniaxial tensile tests with $\sigma_x : \sigma_y = 1{:}0$ and 0:1. For the biaxial stress tests true stress increments were controlled and applied to the specimens so that the von Mises equivalent plastic strain rate became approximately constant at $5\times10^{-4}$ s$^{-1}$ for all stress paths. Two specimens were used for each stress ratio.

The concept of the contour of plastic work in the stress space [23, 24] was used to quantitatively evaluate the work hardening behavior of the test material under biaxial tension. The stress-strain curve obtained from a uniaxial tensile test in the RD was selected as a reference datum for work hardening; the uniaxial true stress $\sigma_0$ and the plastic work per unit volume $W_0$, associated with a particular value of a true plastic strain $\varepsilon_0^p$, were determined. The uniaxial true stress $\sigma_{90}$ in the TD and the biaxial true stress components $(\sigma_x, \sigma_y)$ were then determined at the same plastic work as $W_0$. The stress points $(\sigma_0, 0)$, $(0, \sigma_{90})$ and $(\sigma_x, \sigma_y)$ thus plotted in the principal stress space form a contour of plastic work associated with $\varepsilon_0^p$. When $\varepsilon_0^p$ is taken as sufficiently small, the corresponding work contour can be practically viewed as a yield locus.

Slight differences in flow stress between the tubular and cruciform specimens were observed for all stress ratios, due to the prestrain applied to the sheet sample during tube fabrication. The prestrain distributes linearly in the thickness direction, where it is 0 at the mid thickness and takes the maximum and minimum values, $\pm t_0 / (D_0 - t_0)$, at the outer and inner surfaces of the tube, respectively; these were ±0.012 for the specimen geometry shown in Fig. 1b. From this reason, the s-s curves measured from the multiaxial tube expansion tests were shifted along the strain axis to find a connecting point at which both s-s curves smoothly connect to those measured using a cruciform specimen for the same stress ratio. Details of the shifting method are given in Kuwabara and Sugawara [17].

## 3. RESULTS OF THE BIAXIAL STRESS TESTS

Figure 2a shows the measured stress points forming the contours of plastic work for different levels of $\varepsilon_0^p$. Each stress point represents an average of two specimen data; the difference of the two measured data was less than 2% of the flow stress for all data points. The maximum value of $\varepsilon_0^p$ for which the work contour has a full set of nine stress points was $\varepsilon_0^p = 0.289$. The work contours for a strain range of $0.002 \le \varepsilon_0^p \le 0.04$ were determined from the data obtained using cruciform specimens, and the work contours for a strain range of $0.04 < \varepsilon_0^p \le 0.289$ were determined from the data obtained using the MTET. For $\sigma_x : \sigma_y = 1:1$ fracture occurred at weld lines of tubular specimens at $\varepsilon_0^p = 0.13$; therefore, the equibiaxial stress-strain curves were measured using the hydraulic bulge tests for $\varepsilon_0^p \ge 0.13$ (see Kuwabara and Sugawara [17] for the detail of the hydraulic bulge testing method).

In Fig. 2b all stress values forming a work contour for a value of $\varepsilon_0^p$ are normalized by the associated value of $\sigma_0$. The normalized work contours showed a tendency of expansion, exemplifying the DH [23, 24].

## 4. MATERIAL MODELING

As described in section 5, the effect of material models on the accuracy of the hole expansion simulation is investigated for selected yield functions: the von Mises [8], Hill's quadratic (Hill'48) [3] and the Yld2000-2d [25, 26] yield functions. The isotropic hardening (IH) model was applied to the von Mises and Hill'48 yield functions, while both IH and DH models were applied to the Yld2000-2d yield function. The procedures for determining unknown parameters

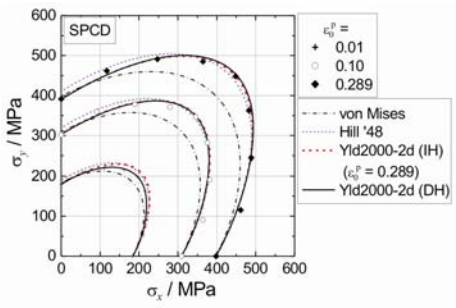


(a)

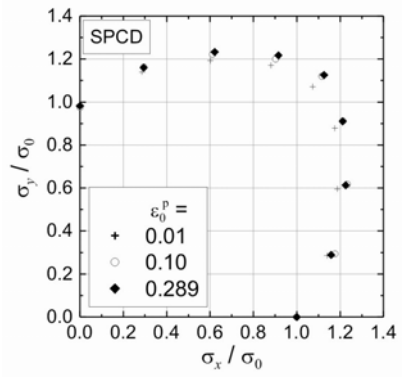


(b)

Fig. 2 – Measured stress points forming contours of plastic work: a) comparison with the theoretical yield loci based on selected yield functions; b) those normalized by the uniaxial tensile stresses $\sigma_0$ associated with different levels of $\varepsilon_0^p$. It is noted in (a) that the yield loci based on the Yld2000-2d (IH) yield function are similar for all the levels of $\varepsilon_0^p$ as the isotropic hardening is assumed.

of Hill's quadratic and the Yld2000-2d yield functions are described in this section. Hereafter, the *r*-value and tensile flow stress measured at θ from the RD, are referred to as $r_\theta$ and $\sigma_\theta$, respectively, and the ratio of the plastic strain rates $d\varepsilon_y^p / d\varepsilon_x^p$ and the flow stress at $\sigma_x : \sigma_y = 1:1$ are referred to as $r_b$ and $\sigma_b$, respectively.

### 4.1. IH MODEL

The unknown parameters of Hill'48 yield function were determined using $r_0$, $r_{45}$ and $r_{90}$ shown in Table 1, and $\sigma_0$. Those of the Yld2000-2d (IH) yield function were determined using $r_0$, $r_{45}$, $r_{90}$ (see Table 1), and $r_b$, $\sigma_0$, $\sigma_{45}$, $\sigma_{90}$ and $\sigma_b$ determined from the work contour for $\varepsilon_0^p = 0.289$ (see Fig. 2): $\sigma_{45}/\sigma_0 = 1.003$, $\sigma_{90}/\sigma_0 = 0.982$, $\sigma_b/\sigma_0 = 1.125$, and $r_b = 0.919$. The value of an exponent *M* (=4.28) was selected to minimize the root mean square error $\delta_r$ between the work contour for $\varepsilon_0^p = 0.289$ and the calculated yield locus (see Eq. (3)). The yield loci calculated using the von Mises, Hill'48, and the Yld2000-2d (IH) yield functions based on the IH model are shown in Fig. 2.

### 4.2. DH MODEL

In order to reproduce the differential hardening behavior of the test material, the contours of plastic work were measured for every $\varepsilon_0^p$ at an increment of 0.01. Then, $\alpha_i$ ($i = 1\sim8$) and *M* of the Yld2000-2d (DH) yield function were determined for respective work contours for $0.002 \le \varepsilon_0^p \le 0.289$ to minimize the root mean square error between the measured work contour and the calculated yield locus, see Eq. (5). Figure 3 shows the variations in $\alpha_i$ and *M* with $\varepsilon_0^p$. The variation of $\alpha_i$ ($i = 1\sim8$) and *M* are relatively large for a strain range of $0.002 \le \varepsilon_0^p \le 0.05$, while they are almost constant for $0.05 < \varepsilon_0^p$.

Moreover, the variations in $\alpha_i$ and *M* with $\varepsilon_0^p$ were approximated by the following equations (see ANNEX for the details on the calculation procedures):

$$M(\varepsilon_0^p) = (A_1 - A_2) / \left[1 + \exp\left\{(\varepsilon_0^p + A_3)/A_4\right\}\right] + A_2, \tag{1}$$

$$\alpha_i(\varepsilon_0^p) = A - B\exp\left(-C\varepsilon_0^p\right) + D/\varepsilon_0^p. \tag{2}$$

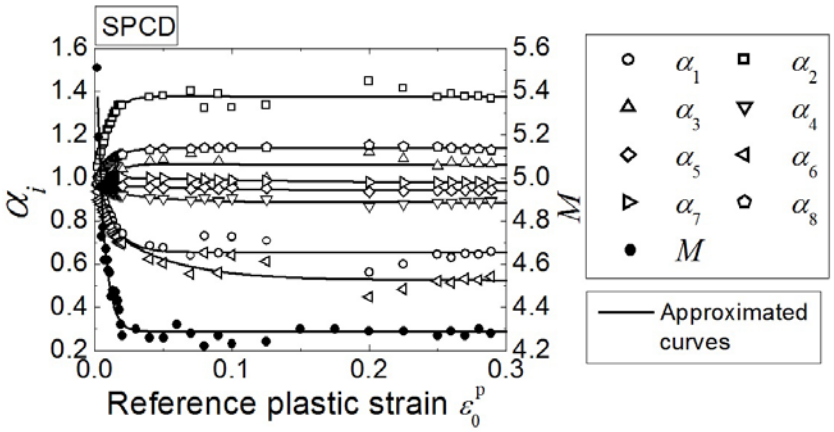


Fig. 3 – Variations of $M$ and $\alpha_i$ with $\varepsilon_0^p$, and those approximated using Eqs. (3) and (4).

The parameters $A_1$, $A_2$, $A_3$ and $A_4$ for $M$, and $A$, $B$, $C$, and $D$ for $\alpha_i$ ($i$=1~8) are listed in Table 2. The approximation curves for $\alpha_i$ ($i$=1~8) and $M$ based on Eqs. (3) and (4) are also shown in Fig. 3. In the FEA of the hole expansion forming the values of $\alpha_i$ ($i$=1~8) and $M$ for the work contours at $0.002 > \varepsilon_0^p$ were assumed to be identical to those for the work contour at $\varepsilon_0^p = 0.002$, so that zero division can be avoided in Eq. (4). It is confirmed from Fig. 3 that the variations of $\alpha_i$ ($i$=1~8) and $M$ with an increase of $\varepsilon_0^p$ are correctly reproduced by Eqs. (3) and (4).

*Table 2*

Parameters of the Yld2000-2d yield function for the DH model

| | $M$ | | $\alpha_1$ | $\alpha_2$ | $\alpha_3$ | $\alpha_4$ |
|---|---|---|---|---|---|---|
| $A_1$ | 76.82151 | $A$ | 0.65589 | 1.3757 | 1.05933 | 0.88623 |
| $A_2$ | 4.28845 | $B$ | –0.44394 | 0.53476 | 0.24348 | –0.06033 |
| $A_3$ | 0.02028 | $C$ | 84.36394 | 119.55826 | 105.04006 | 24.48797 |
| $A_4$ | 0.00532 | $D$ | –0.00006 | 0.0002 | 0.00025 | 0.00003 |
| | | | $\alpha_5$ | $\alpha_6$ | $\alpha_7$ | $\alpha_8$ |
| | | $A$ | 0.94017 | 0.52442 | 0.97626 | 1.138 |
| | | $B$ | –0.02893 | –0.27252 | –0.03193 | 0.1748 |
| | | $C$ | 12.02196 | 21.76577 | 7.95456 | 100.1 |
| | | $D$ | $6.863\times10^{-7}$ | 0.00037 | –0.00005 | –0.00005 |

*Approximated using $M(\varepsilon_0^p) = (A_1 - A_2) / \left[1 + \exp\left\{(\varepsilon_0^p + A_3) / A_4\right\}\right] + A_2$ for $0.002 \le \varepsilon_0^p \le 0.289$.

**Approximated using $\alpha_i = A - B\exp\left(-C\,\varepsilon_0^p\right) + D / \varepsilon_0^p$ for $0.002 \le \varepsilon_0^p \le 0.289$.

## 4.3. VALIDATION OF THE MATERIAL MODELS

The theoretical yield loci based on the von Mises (IH model), Hill'48 (IH model) and the Yld2000-2d yield function (IH and DH models) are superimposed in Fig. 2a. To quantitatively evaluate the difference between the shapes of the theoretical yield loci and the measured work contours, the root mean square error $\delta_r$ was calculated using the following equation:

$$\delta_r = \sqrt{\frac{\sum_i \{r'(\varphi_i) - r(\varphi_i)\}^2}{N}}, \tag{3}$$

where $\varphi_i$ ($i = 1$ to $N$ (=9)) is the loading angle of the $i$-th stress path from the $x$-axis in the principal stress space, $r(\varphi_i)$ is the distance between the origin of the principal stress space and the $i$-th stress point, and $r'(\varphi_i)$ is the distance between the origin of the principal stress space and the theoretical yield locus along the loading direction $\varphi_i$ (see the schematic in Fig. 4). Figure 4 shows the values of $\delta_r$ for the work contours at $\varepsilon_0^p = 0.01$, 0.10, and 0.289. It is clear that the Yld2000-2d (DH) yield function gives the most accurate description of the work hardening behavior of the test material, although there is not much difference in $\delta_r$ between Hill'48, the Yld2000-2d (IH), and the Yld2000-2d (DH) yield functions.

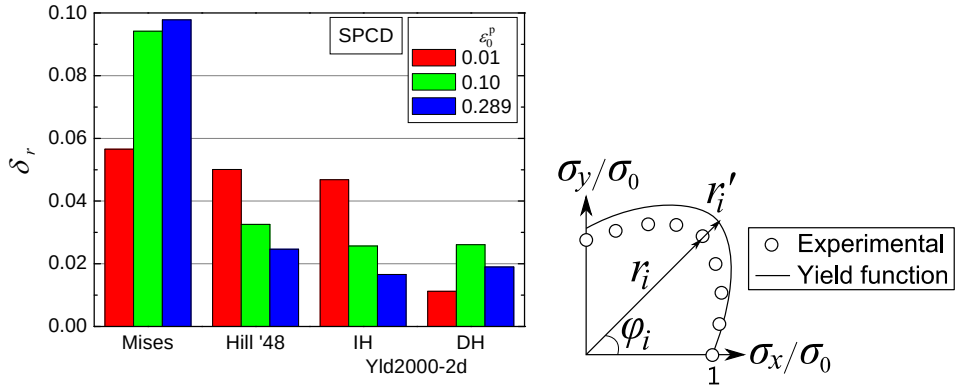


Fig. 4 – The root mean square error $\delta_r$ of the calculated yield loci from the measured work contours associated with $\varepsilon_0^p = 0.01$, 0.10, and 0.289.

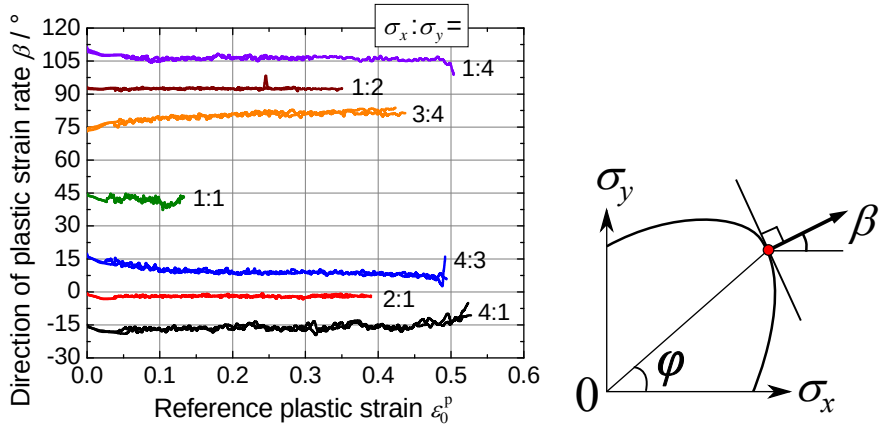


Fig. 5 – Variation of the directions of the plastic strain rates with $\varepsilon_0^p$.

In order to validate the normality flow rule for the yield functions, the directions of the plastic strain rates were measured for each linear stress path. Figure 5 shows the variation of the directions β of the plastic strain rates with an increase of $\varepsilon_0^p$ for each linear stress path. β is defined as 0° when it is parallel to the RD, and the increment of β in the anticlockwise direction is defined to be positive. β is almost constant for $\sigma_x:\sigma_y = 4:1$, 2:1, 1:1, 1:2, and 1:4, while β gradually decreases for $\sigma_x:\sigma_y = 4:3$ and increases for $\sigma_x:\sigma_y = 3:4$ with an increase of $\varepsilon_0^p$.

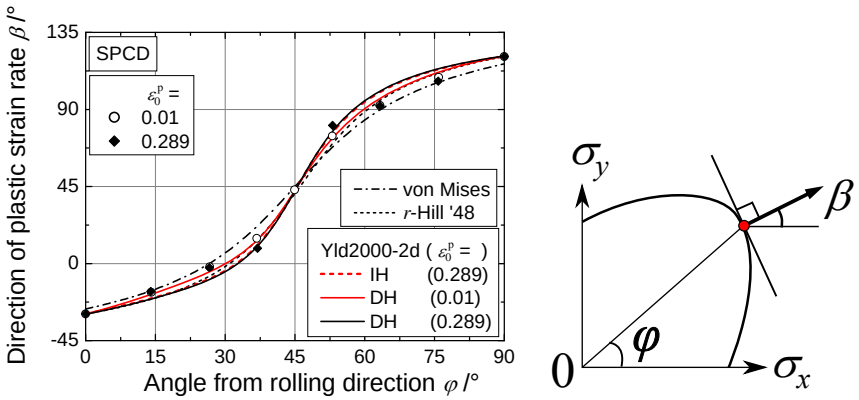


Fig. 6 – Directions of the plastic strain rates measured at $\varepsilon_0^p = 0.01$ and 0.289, compared with those calculated using selected yield functions.

Figure 6 compares the measured directions of the plastic strain rates measured at $\varepsilon_0^p = 0.01$ and 0.289 with those calculated using selected yield functions based on the IH model and the Yld2000-2d (DH) yield function.

To quantitatively evaluate the difference between the measured directions of the plastic strain rates and those predicted using the selected yield functions, the root mean square error $\delta_\beta$ was calculated using the following equation:

$$\delta_\beta = \sqrt{\frac{\sum_i \{\beta'(\varphi_i) - \beta(\varphi_i)\}^2}{N}}, \tag{4}$$

where $\beta(\varphi_i)$ ($i = 1 \sim N$ (=9)) is the direction of the plastic strain rate measured for the $i$-th stress path, and $\beta'(\varphi_i)$ is that predicted using a selected yield function for the $i$-th stress path (see the schematic in Fig. 7). Figure 7 shows the values of $\delta_\beta$ for the work contours at $\varepsilon_0^p = 0.01$, 0.10, and 0.289. The Yld2000-2d yield function (DH) gives the most accurate prediction of $\beta(\varphi_i)$ at $\varepsilon_0^p = 0.01$, while there is not much difference in $\delta_\beta$ between Hill'48, the Yld2000-2d (IH), and the Yld2000-2d (DH) yield functions at higher strain levels of $\varepsilon_0^p = 0.10$ and 0.289.

Figure 8 compares the measured uniaxial tensile stresses $\sigma_\theta$ (normalized by $\sigma_0$) and the $r$-values $r_\theta$ corresponding to $\varepsilon_0^p = 0.095$, for a loading angle of $\theta$ from the RD, with the calculated values using the yield functions examined in this study. The Yld2000-2d yield function has a good agreement with the experimental values for both $\sigma_\theta$ and $r_\theta$, while the values of $\sigma_\theta$ predicted by Hill'48 show some deviation from the measurement.

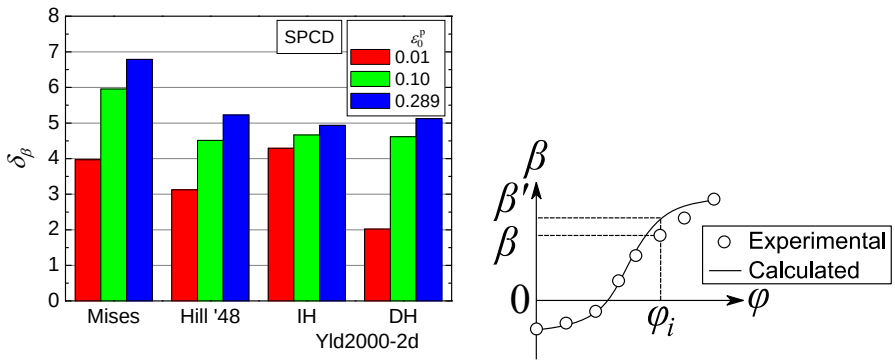


Fig. 7 – The root mean square error $\delta_\beta$ of the calculated directions of the plastic strain rates based on the normality flow rule for the calculated yield locus from those measured.

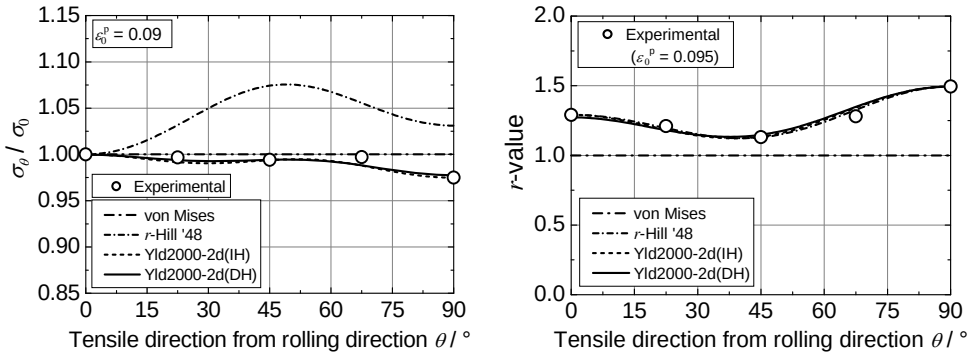


Fig. 8 – Variation of: a) flow stresses; b) *r*-values with tensile directions, compared with those calculated using the selected yield functions.

## 5. HOLE EXPANSION FORMING: EXPERIMENT AND FINITE ELEMENT SIMULATION

### 5.1. EXPERIMENTAL METHOD

Figure 9 shows the experimental apparatus used for the hole expansion forming. The punch was 100 mm in diameter and the die and punch profile radius was 15 mm. The initial hole diameter was 30 mm, fabricated at the center of a circular blank using a wire-electrical discharging machine. The periphery of the blank was clamped using a triangular draw-bead. The interface between the blank and punch head was lubricated with Vaseline and 0.3 mm thick Teflon sheet. The punch speed was approximately 0.1 mm/s, and the punch stroke was 30 mm. A grid pattern, with an increment of 10° in the circumferential direction and 2 mm in the radial direction, was scribed on each blank. The grid was used to identify the initial position of each material element in the original sheet when the thickness strain distribution in the sheet was measured after a hole expansion forming.

After the hole expansion forming, the sheet thickness along the hole edge (at positions 2 mm distant from the hole edge on the undeformed blank) and along the radial lines at 0, 45, 90, 135, 180, 225, 270, 315° from the RD were measured using a digital micrometer with a minimum readout of 0.001 mm.

### 5.2. FINITE ELEMENT ANALYSIS

FEAs of the hole expansion forming were carried out using Abaqus/Standard Ver.6.12 [27]. Figure 10a shows the finite element mesh used for the analysis. The increment of element divisions in the circumferential direction was 2.5°. The

increment of element division in the radial direction was 1 mm for $15 \le R \le 69$ mm, 1.5 mm for $69 \le R \le 82.5$ mm, and 2 mm for $82.5 \le R \le 97.5$ mm, where $R$ is the radial coordinate on the undeformed blank. One quarter of a blank was analyzed, due to the orthotropic material symmetry. The reduced 4-node shell elements (S4R) with 5 integration points in the thickness direction were used for the blank.

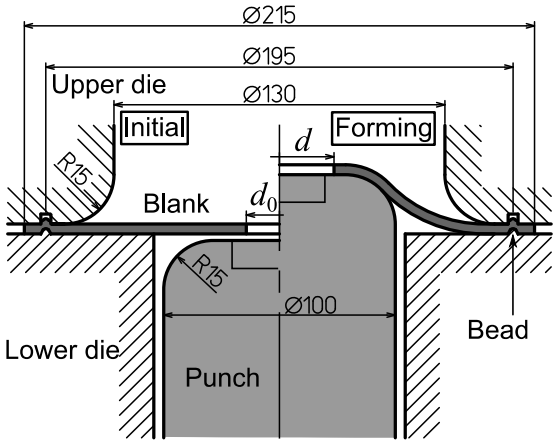


Fig. 9 – Experimental apparatus for the hole expansion forming.

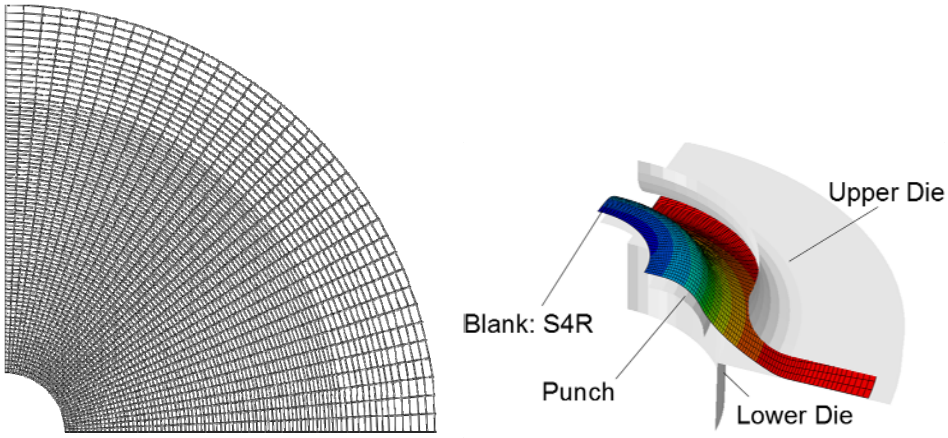


(a) (b)

Fig. 10 – Finite element analysis of the hole expansion forming: a) initial mesh division of a blank; b) the FEA model for the hole expansion forming.

The initial hole diameter was 30 mm. The punch, die, and blank-holder were defined as rigid bodies, as shown in Fig. 10b. The coefficients of friction were assumed to be 0.03 between the punch and blank and 0.15 for other contact areas of the blank. The displacement of the blank edge (a diameter of 195 mm) was fixed at the bead position. Swift's power law in the RD shown in Table 1 was used as the

work hardening equation of the material. The material was unloaded when the punch stroke reached 30 mm, and the FEA was terminated.

The material models used in the FEA were the IH models based on the von Mises, Hill'48 and the Yld2000-2d (IH) yield functions (see Fig. 2a). In addition, the DH model (the Yld2000-2d (DH)) as formulated in section 4.2 was also used.

## 5.3 RESULTS AND DISCUSSION

Figure 11 compares the measured logarithmic thickness strains $\varepsilon_z^p$ along the hole edge (the positions 2 mm away from the hole edge on the undeformed blank) at a punch stroke $h = 30$ mm with the FEA predictions calculated using selected yield functions. One data point indicates an average value of three specimens. In the figure, the hole expansion ratio λ is defined as

$$\lambda \equiv \frac{C - C_0}{C_0}, \tag{5}$$

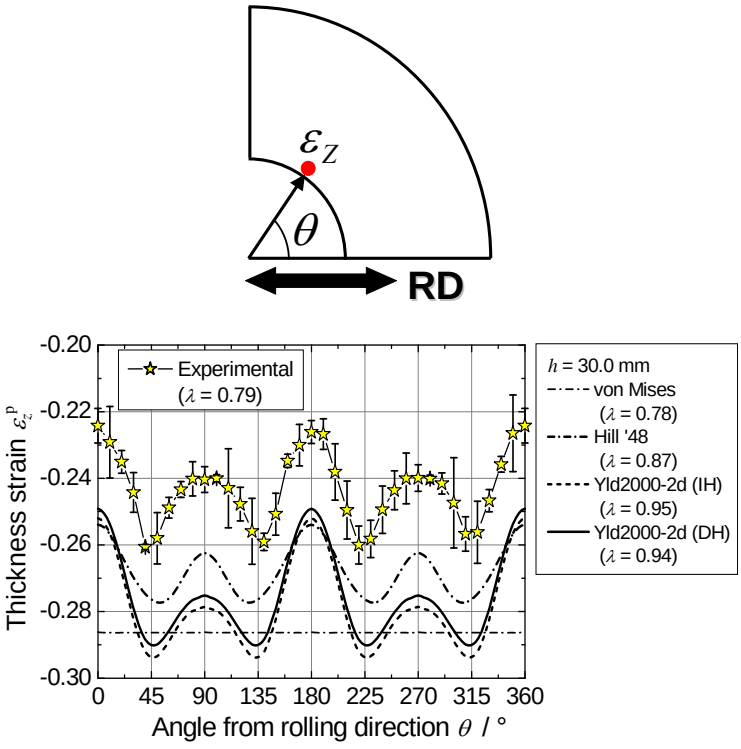


Fig. 11 – Thickness strains along the expanded hole edge compared with those calculated using selected yield functions. The punch stroke in the experiment and the FEA was 30 mm.

where $C_0$ and $C$ are the total length of the hole edge before and after the hole expansion forming. The experimental data had local maxima at $\theta = 0$, 90, 180 and 270° and local minima at $\theta = 45$, 135, 225 and 315°. All the material models overestimate the thickness reduction along the hole edge. Taking a closer look at the FEA predictions, the Yld2000-2d (IH) and (DH) correctly predict the directions of local maxima and minima, while Hill'48's prediction slightly deviates from the measurement. The difference between the maxima and minima in the experimental thickness strain was 0.033, while those in the FEA results were 0.022 for Hill'48, 0.042 for the Yld2000-2d (IH), 0.041 for the Yld2000-2d (DH) and 0 for the von Mises yield function.

Figure 12 shows the variation of $\varepsilon_z^p$ measured along the radial lines at the RD (average of $\theta = 0$ and 180°), 45° (average of $\theta = 45$, 135, 225 and 315°), and the TD (average of $\theta = 90$ and 270°), compared with the FEA predictions calculated using the von Mises (a), Hill's quadratic (b), and the Yld2000-2d (DH) (c) yield functions, respectively. The horizontal axis indicates the strain measurement position that is $S$ mm away from the hole edge on the undeformed blank. The measured $\varepsilon_z^p$ takes the minimum approximately at $S = 10$ mm for $\theta = 0$ and 90° and at $S = 8$ mm for $\theta = 45°$. The calculated values using Yld2000-2d (DH) yield function are in fair agreement with the measurement for a range of $14 \le S \le 20$ mm; however it could not predict the trend that $|\varepsilon_z^p|$ increases with an increase of $S$ for a range of $2 \le S \le 10$ mm at $\theta = 0$ and 90° and for a range of $2 \le S \le 8$ mm at $\theta = 45°$. On the other hand, the calculated values using Hill'48 show a deviation of $\Delta\varepsilon_z^p = 0.01 \sim 0.04$ from the measurement, although it coincidentally predicts the trend that $\varepsilon_z^p$ takes the minimum approximately at $S = 10$ mm for the RD and TD.

It is clear from Fig. 12 that all the material models could not accurately reproduce the $|\varepsilon_z^p|$ distribution in the vicinity of the hole edge, i.e., in the area of $0 \le S \le 12$ mm. The stress states of the material elements existing in this area change from uniaxial tension (at $S = 0$) to plane strain tension (in the vicinity of $S = 12$ mm. Actually, the directions of the plastic strain rates at $\sigma_x : \sigma_y = 4{:}1$, 2:1, 1:2, and 1:4 predicted by the Yld2000-2d yield function (DH) deviate from the measurement by several degrees as shown in Fig. 6. Therefore, in order to improve the predictive accuracy for the thickness distribution in the vicinity of the hole edge, a material model that accurately reproduces the anisotropic deformation behavior of the test material for a stress range from uniaxial tension to plane strain tension along the RD, 45°, and TD should be used in the FEA. The development of such an accurate material model will be an objective for a future study.

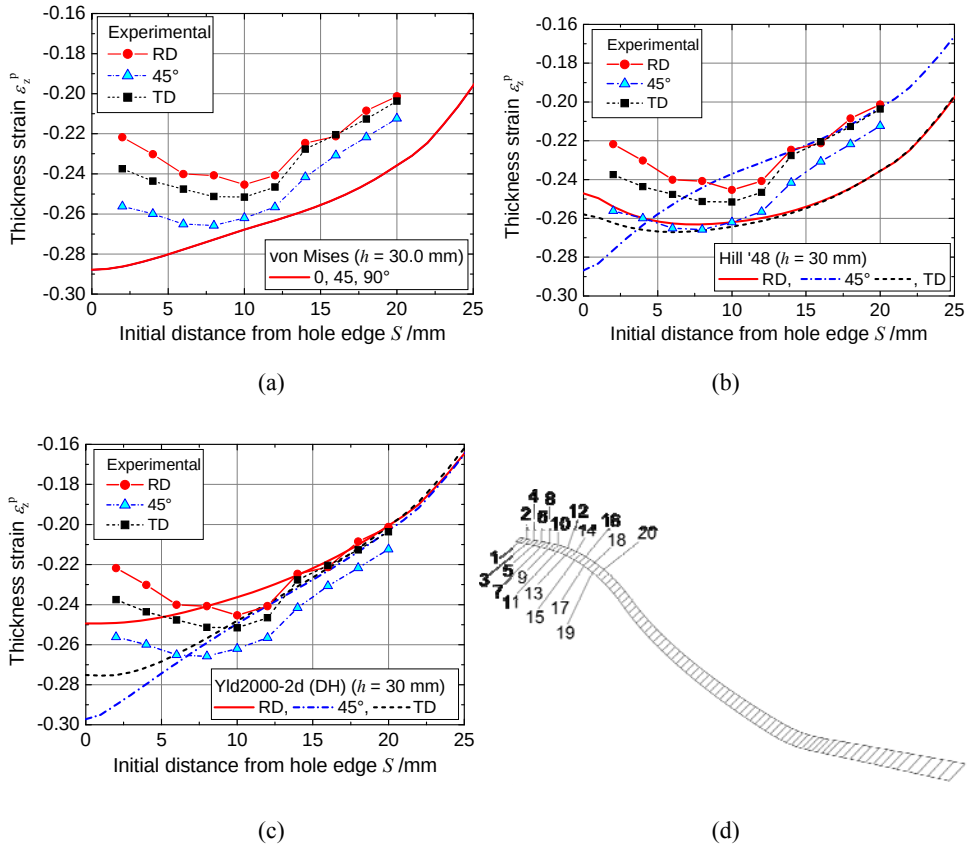


Fig. 12 – Measured thickness strains along the radial lines parallel to the RD, 45°, and TD of the blank at a punch stroke of 30 mm. Also depicted in these figures are those calculated using: a) the von Mises; b) Hill'48; c) the Yld2000-2d (DH) yield functions, respectively; d) a law of deformed elements at $h = 30$ mm. The numerals indicate the initial distance $S$ (mm) from the hole edge.

## 6. CONCLUSIONS

FEAs of hole expansion forming of a zinc-coated low carbon steel sheet (SPCD) were performed using the material models that were precisely determined using the data from the biaxial tensile tests using cruciform specimens and the MTET. The material models used in the FEA were the IH models based on the von Mises, Hill'48 and the Yld2000-2d yield functions and the DH model based on the Yld2000-2d yield function. Calculated thickness strain distributions in the vicinity of the hole edge were compared with experimental data, and the cause of the discrepancy between the experiment and the FEA was discussed. The following conclusions were obtained.

(1) The DH model based on the Yld2000-2d yield function gives the most accurate description of the biaxial deformation behavior of the test material in terms of contours of plastic work and the normality flow rule, although it does not have much difference in accuracy at a higher strain range from the IH models based on Hill'48 and the Yld2000-2d yield functions.
(2) Even the DH model based on the Yld2000-2d yield function could not accurately reproduce a tendency of $\varepsilon_z^p$ distribution that $|\varepsilon_z^p|$ increases with an increase of the distance $S$ from the hole edge for a range of $2 \le S \le 10$ mm at $\theta = 0$ and 90° and for a range of $2 \le S \le 8$ mm at $\theta = 45°$.
(3) In order to improve the predictive accuracy for the thickness distribution in the vicinity of the hole edge, a material model that accurately reproduces the anisotropic deformation behavior of the test material for a stress range from uniaxial tension to plane strain tension along the RD, 45°, and TD should be used in the FEA.

## ANNEX

In order to formulate the differential hardening model for the test material, the material parameters $\alpha_i$ ($i = 1 \sim 8$) and exponent $M$ of the Yld2000-2d yield function were determined as functions of $\varepsilon_0^p$ by the following calculation procedures:

(i) $\alpha_i$ ($i = 1 \sim 8$) and $M$ of the Yld2000-2d yield function were determined for respective work contours for $0.002 \le \varepsilon_0^p \le 0.289$ to minimize the root mean square error between the measured work contour and the calculated yield locus, see Eq. (3).
(ii) Approximate the variation in $M$ with $\varepsilon_0^p$ using Eq. (1).
(iii) Recalculate $\alpha_i$ ($i = 1 \sim 8$) using the value of $M$ determined in (ii) for the measured work contours corresponding to particular values of $\varepsilon_0^p$.
(iv) Approximate the variations in $\alpha_i$ ($i = 1 \sim 8$) with $\varepsilon_0^p$ obtained in (iii) using Eq. (2).

*Received on June 29, 2015*

## REFERENCES

1. KUWABARA, T., *Biaxial Stress Testing Methods for Sheet Metals*, in: *Comprehensive Materials Processing* – Vol. 1 (ed. C.J. Van Tyne), 2014, Elsevier Ltd. , pp. 95–111.
2. PARMAR, A., MELLOR, P.B., *Plastic expansion of a circular hole in sheet metal subjected to biaxial tensile stress*, Int. J. Mech. Sci., **20**, *10*, pp. 707–720, 1978.

3. HILL, R., *Theoretical plasticity of textured aggregates*, Math. Proc. Camb. Phil. Soc., **85**, *1*, pp. 179-191, 1979.
4. TAKUDA, H., OZAWA, K., HAMA, T., YOSHIDA, T., NITTA, J., *Forming limit prediction in bore expansion by combination of finite element simulation and ductile fracture criterion*, Mater. Trans., **50**, pp. 1930–1934, 2009.
5. HILL, R., *A theory of the yielding and plastic flow of anisotropic metals*, Proc. Roy. Soc. London A, **193**, pp. 281–297, 1948.
6. WORSWICK, M.J., FINN, M.J., *The numerical simulation of stretch flange forming*, Int. J. Plasticity, **16**, *6*, pp. 701–720, 2000.
7. BARLAT, F., LIAN, K., *Plastic behavior and stretchability of sheet metals. Part I: A yield function for orthotropic sheets under plane stress conditions*, Int. J. Plasticity, **5**, *1*, pp. 51–66, 1989.
8. VON MISES, R., *Mechanik der festen Korper un plastich deformablen Zustant*, Göttingen Nachrichten, math.-phys. Klasse, pp. 582–592, 1913.
9. KUWABARA, T., IKEDA, S., KURODA, T., *Measurement and analysis of differential work-hardening in cold-rolled steel sheet under biaxial tension*, J. Mater. Process Technol., **80–81**, pp. 517–523, 1998.
10. KUWABARA, T., KURODA, M., TVERGAARD, V., NOMURA, K., *Use of abrupt strain path change for determining subsequent yield surface: experimental study with metal sheets*, Acta Mater., **48**, *9*, pp. 2071–2079, 2000.
11. MORIYA, T., KUWABARA, T., KIMURA, S. and TAKAHASHI, S., *Effect of anisotropic yield function on the predictive accuracy of surface deflection of automotive outer panels*, Steel Res. Int., **81**, 1384–1387, 2010.
12. YANAGA, D., KUWABARA, T., UEMA, N., ASANO, M., *Material modeling of 6000 series aluminum alloy sheets with different density cube textures and effect on the accuracy of finite element simulation*, Int. J. Solids and Struct., **49**, *25*, pp. 3488–3495, 2012.
13. HASHIMOTO, K., KUWABARA, T., IIZUKA, E., YOON, J.W., *Effect of anisotropic yield functions on the accuracy of hole expansion simulations for 590 MPa grade steel sheet* (in Japanese), Tetsu-to-Hagané, **96**, pp. 557–563, 2010.
14. KUWABARA, T., HASHIMOTO, K. IIZUKA, E., YOON J.W., *Effect of anisotropic yield functions on the accuracy of hole expansion simulations*, J. Mater. Processing Technol., **211**, pp. 475–481, 2011.
15. KUWABARA, T., ISHIKI, M., KURODA, M., TAKAHASHI, S., *Yield Locus and Work-Hardening Behavior of a Thin-Walled Steel Tube Subjected to Combined Tension-Internal Pressure*, J. de Physique IV, **105**, pp. 347–354, 2003.
16. ISHIKI, M., KUWABARA, T., HAYASHIDA, Y., *Measurement and analysis of differential work hardening behavior of pure titanium sheet using spline function*, Int. J. Mater. Forming, **4**, *2*, pp. 193–204, 2011.
17. KUWABARA, T., SUGAWARA, F., *Multiaxial tube expansion test method for measurement of sheet metal deformation behavior under biaxial tension for a large strain range*, Int. J. Plasticity, **45**, pp. 103–118, 2013.
18. HAKOYAMA, T., KUWABARA, T., *Effect of biaxial work hardening modeling for sheet metals on the accuracy of forming limit analyses using the Marciniak–Kuczyński approach*, (Chap. 12. in: *From Creep Damage Mechanics to Homogenization Methods* (eds. H. Altenbach, T. Matsuda, D. Okumura), Springer, 2015, pp. 69–96.
19. YANAGA, D., TAKIZAWA, H., KUWABARA, T, *Formulation of Differential Work Hardening of 6000 Series Aluminum Alloy Sheet and Application to Finite Element Analysis* (in Japanese), J. JSTP, **55**, pp. 55–61, 2014.
20. **** Metallic materials — Sheet and strip — Biaxial tensile testing method using cruciform specimen*, ISO 16842.
21. HANABUSA, Y., TAKIZAWA, H., KUWABARA, T., *Evaluation of accuracy of stress measurements determined in biaxial stress tests with cruciform specimen using numerical method*, Steel Res. Int., **81**, pp. 1376–1379, 2010.

22. HANABUSA, Y., TAKIZAWA, H., KUWABARA, T., *Numerical verification of a biaxial tensile test method using a cruciform specimen*, J. Mater. Processing Technol., **213**, pp. 961–970, 2013.
23. HILL, R., HUTCHINSON, J.W., *Differential hardening in sheet metal under biaxial loading: a theoretical framework*, J. Appl. Mech., **59**, *2S*, pp. S1-S9, 1992.
24. HILL, R., HECKER, S.S., STOUT, M.G., *An investigation of plastic flow and differential work hardening in orthotropic brass tubes under fluid pressure and axial load*, Int. J. Solids Struct., **31**, *21*, pp. 2999–3021, 1994.
25. BARLAT, F., BREM, J.C., YOON, J.W., CHUNG, K, DICK, R.E., LEGE, D.J., POURBOGHRAT, F., CHOI, S.H., CHU, E., *Plane stress yield function for aluminum alloy sheets –part 1: theory*, Int. J. Plasticity, **19**, *9*, pp. 1297–1319, 2003.
26. YOON, J.W., BARLAT, F., DICK, R.E., CHUNG, K., KANG, T.J., *Plane stress yield function for aluminum alloy sheets – part II: FE formulation and its implementation*, Int. J. Plasticity, **20**, *3*, pp. 495–522, 2004.
27. ***Abaqus Documentation*, Version 6.12, Dassault Systèmes, 2012.